Journal of Statistical Physics, Vol. 29, No. 1, 1982

Mode Selection in a Caricature of Eutectic Solidification

V. Datye,[1] R. Mathur,[1,2] and J. S. Langer[1,3]

Received March 22, 1981

We have studied the problem of mode selection, specifically, selection of the lamellar spacing, in eutectic solidification, by constructing a caricature of a thin-film eutectic solidifying at constant velocity in the presence of a finite-temperature gradient and in a slightly noisy environment. Our model incorporates mechanisms which allow termination of substable lamellae and creation of new lamellae by the splitting of lamellae larger than a spacing λ_{max}. We have studied this model both by a simple analytic approximation and by computer simulation. We find that both the steady state spacing and the regularity of the pattern are sensitively dependent on the ratio $\lambda_{max}/\lambda_{min}$, where λ_{min} is the minimum spacing required for steady state stability. An additional result to emerge from our investigation is that when λ_{max} becomes less than a critical value, the system apparently undergoes a transition into a chaotic state.

KEY WORDS: Eutectic; mode selection; directional solidification; fluctuations; marginal stability.

1. INTRODUCTION

Directional solidification of a binary fluid near its eutectic composition often produces an alternating parallel array of lamellae of the two coexisting solid phases.[1),4] The central question in the theory of this process is the way in which the system selects its mode of growth, specifically, its lamellar spacing. Related questions pertain to fluctuations in the spacing, the frequency of defects, and the existence of oscillatory or other more complex growth forms. The conventional assumption in the metallurgical literature

[1] Physics Department, Carnegie-Mellon University, Pittsburgh, Pennsylvania 15213.
[2] Present address: Intel Corporation, 3065 Bowers Avenue, Santa Clara, California 95051.
[3] Present address: Institute for Theoretical Physics, University of California, Santa Barbara, California 93106.
[4] For a review of the eutectic problem see Ref. 2.

0022-4715/82/0900-0001$03.00/0

is that eutectic arrays growing at fixed velocity choose the lamellar spacing which minimizes the undercooling at the solidification front. Equivalently, an array growing at fixed temperature is assumed to maximize its velocity. We have shown in recent publications[3–5] that these growth criteria are equivalent to a principle of marginal stability which states that the system will operate at a point where it is just on the verge of being unstable against fluctuations which tend to change its spacing. These equivalent hypotheses predict a relation of the form

$$\lambda^2 v = \text{const} \tag{1.1}$$

where λ is the lamellar spacing, v is the growth velocity, and the constant on the right-hand side is a well-defined function of the properties of the solidifying material—interfacial tensions, diffusion constants, etc. The functional form of (1.1) has been verified experimentally[6] but, to our knowledge, the value of the constant has never been checked by independent measurements of its various ingredients.

There exists no truly compelling argument in favor of the minimum-undercooling–marginal-stability hypothesis. Our intuitive argument for marginal stability, that the system drifts toward the instability because fluctuations tending in that direction persist for longer times than those that go the other way, does not preclude situations in which other forces or constraints are dominant. Because of this uncertain theoretical situation, it seems useful to study very simplified models of eutecticlike pattern-forming systems, if only to gain some qualitative understanding of what kinds of mode-selection mechanisms are possible.

Accordingly, in what follows we consider a mode-selection model which has some, but by no means all, of the essential features of the eutectic solidification problem. This euctectic caricature is based on a nonlinear partial differential equation derived previously by one of us (JSL)[3] in an analysis of eutectic growth near the marginal-stability point. The caricature is intended to resemble, very crudely, a thin-film eutectic solidifying at constant velocity with a finite-temperature gradient at the solidification front and in a slightly noisy environment. In addition to the diffusion kinetics described by the basic equation of motion, we introduce into our model mechanisms which allow substable lamellae to terminate and new lamellae to form, the latter process occurring by splitting of lamellae which have grown too wide. The ratio of the maximum lamellar width, λ_{max}, to the minimum width required for stability, λ_{min}, turns out to be the dimensionless parameter which, along with the noise strength, controls the qualitative behavior of our model—its average spacing and the regularity of the lamellar pattern.

We have studied this model both by a simple analytic approximation and by computer simulation. As will be apparent in our description of these studies, this model does not generally select its steady mode of operation

near the marginal-stability point. Rather, when λ_{max} is appreciably greater than λ_{min}, and when the noise strength is not too large, the average spacing occurs roughly halfway between λ_{max} and λ_{min}. As the noise strength increases, the spacing shifts toward λ_{min}; and this shift is all that remains of the marginal-stability principle. Apparently the system is too highly constrained for this principle to have a dominant effect; the mechanisms for changing the lamellar spacing—splittings and terminations—require perturbations of the system which are too large and discontinuous to permit the drift toward instability that seems to occur, for example, in dendritic systems.

One specially interesting result to emerge from our investigation is that, when λ_{max} decreases toward λ_{min}, the system apparently undergoes a transition into a chaotic state. That is, even in the absence of external noise, the system exhibits spatially and temporally persistent, irregular motion. We believe that behavior of this kind has been seen experimentally.[7]

The scheme of this paper is as follows. Our eutectic caricature is described in Section 2. Section 3 is devoted to a simple "mean-field" approximation for the system which, while very crude, provides some insight regarding both the mechanisms for mode selection and the transition to chaotic behavior. The computer simulations are described in Section 4.

2. DEFINITION OF THE MODEL

The starting point of our investigation is an approximate equation of motion [5] for the lamellar width λ at a position x along the solidification front of a eutectic array (see Fig. 1). This equation has the form

$$\frac{\partial \lambda}{\partial t} \cong \frac{v\lambda}{G} \frac{\partial^2}{\partial x^2} \Delta T(\lambda) \tag{2.1}$$

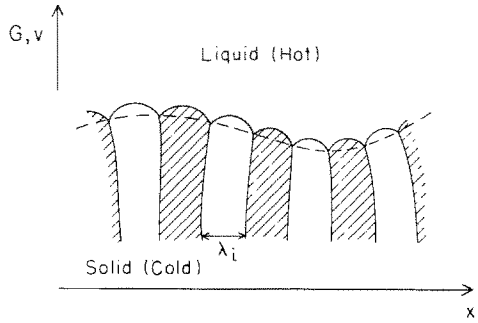

Fig. 1. Schematic illustration of a lamellar eutectic undergoing directional solidification in the z direction with velocity v, in the presence of a thermal gradient, G. The lamellar widths λ_i are shown.

where v is the growth velocity, G the temperature gradient, and $\Delta T(\lambda)$ the Jackson–Hunt[1] relation between λ and the undercooling ΔT (measured from the eutectic temperature T_E) at the liquid–solid interface. Equation (2.1) can be understood qualitatively by noting that $\Delta T/G$ is the position of the solidification front in the imposed thermal field, thus the right-hand side is approximately proportional to the curvature of this front. If the lamellae grow at velocity v normal to the front, then (2.1) describes how their widths decrease as they converge in a region of positive curvature or similarly increase where the curvature is negative. The equation, as written, is valid only in the case of a substantial temperature gradient G moving with the front and oriented in the direction of growth, so that curvatures are expected to be small and the overall orientation of the front is fixed.

The function $\Delta T(\lambda)$ has the form

$$\Delta T = \frac{1}{2}\Delta T_{\min}\left(\frac{\lambda}{\lambda_{\min}} + \frac{\lambda_{\min}}{\lambda}\right) \tag{2.2}$$

Here, $\lambda_{\min}$ has the characteristic form of a stability length; that is,

$$\lambda_{\min} \propto (Dd_0/v)^{1/2} \tag{2.3}$$

is the geometric mean of a capillary length d_0 and the diffusion length D/v, where D is the diffusion constant in the fluid. The temperature $\Delta T_{\min}$ is proportional to the dimensionless group of parameters $(d_0 v/D)^{1/2}$. For our purposes, the important feature of ΔT is that it passes through a minimum as a function of λ at $\lambda = \lambda_{\min}$, $\Delta T = \Delta T_{\min}$.

Equation (2.1), by itself, does not contain enough of the detailed lamellar dynamics to be a complete model of mode selection. As was pointed out in Ref. 3, this equation describes the onset of instabilities which lead to terminations of lamellae; but it does not tell us how the system recovers from such events, nor does it tell us how new lamellae might be formed. Both of the latter mechanisms will be necessary ingredients of any model that will permit us to study, for example, how a lamellar array emerges from an initially irregular configuration or adjusts to subsequent perturbations.

The mathematical model that we have chosen to investigate—our eutectic "caricature"—is based crudely on (2.1) and contains the termination and creation mechanisms in a way which is very simple but not entirely unrealistic. It is described by the following set of coupled nonlinear differential equations:

$$\frac{\partial \Lambda i}{\partial \tau} = (\Lambda_{i+1} - 1)^2 - 2(\Lambda_i - 1)^2 + (\Lambda_{i-1} - 1)^2 + \eta_i - \eta_{i-1}, \qquad 0 \leqslant \Lambda_i \leqslant \Lambda_{\max} \tag{2.4}$$

Here, Λ_i may be thought of as the width of the ith lamella measured in

units of $\lambda_{\min}$, τ is a timelike variable, and η_i is a random force to be specified below. Note that the Λ-dependent part of the right-hand side of (2.4) is a finite-difference approximation for right-hand side of (2.1) with the original λ dependence of ΔT as given in (2.2) replaced by a simple quadratic minimum at $\Lambda = 1$. The noise η is chosen so that

$$\langle \eta_i(t)\eta_j(t') \rangle = \theta \delta_{ij} \delta(t - t') \tag{2.5}$$

where the angular brackets denote a statistical average and θ is an effective temperature. (We believe that thermal fluctuations are much too small to play any role in mode selection, and suspect that the important sources of noise are irregularities in the walls of the container or other macroscopic inhomogeneities.) The η's have been inserted into (2.4) in such a way that the total width of the system is conserved. It will be convenient in later numerical work to impose reflecting boundary conditions at the edges of the system; that is, $\Lambda_{-1} = \Lambda_1$, $\Lambda_{N+1} = \Lambda_{N-1}$, and $\eta_0 = \eta_N$. Then

$$L \equiv \sum_{i=1}^{N-1} \Lambda_i + \tfrac{1}{2}(\Lambda_0 + \Lambda_N) \tag{2.6}$$

is a constant of the motion, even in the presence of the noise.

The most natural way to introduce lamellar terminations and creations for a eutectic with roughly equal volume fractions of the two solid phases—the physical situation to which our model is most nearly applicable—would be to define transition rules as illustrated in Fig. 2a. Specifically, whenever

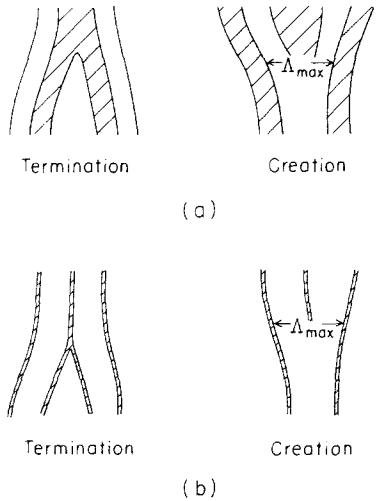

Fig. 2. Schematic illustration of termination and creation of lamellae. (a) Equal volume fractions. (b) Highly unequal volume fractions. The version used in this paper corresponds to case (b).

some Λ_i vanishes, that lamella is removed from the system, and the two neighboring lamellae are combined to form a single one at that position. Whenever some Λ_i exceeds a predetermined Λ_{max}, that lamella is split into three new ones of width $\Lambda_i/3$. This mechanism, however, is slightly inconvenient for technical reasons; and, because our caricature is not intended to be very realistic in any case, we have chosen to work with the simpler version shown in Fig. 2b. We have drawn Fig. 2b so as to suggest that the volume fractions of the solid phases are far from equal and that the Λ_i refer only to the widths of majority-phase lamellae. Here, a termination occurs when some Λ_i vanishes, but the two neighboring lamellae continue on as before. A splitting occurs when some Λ_i exceeds Λ_{max}; but now just two lamellae appear with widths $\Lambda_i/2$.

The quantity $\Lambda_{max} = \lambda_{max}/\lambda_{min}$ has become the principal control parameter in this system. Jackson and Hunt[1] have attempted a first-principles calculation of λ_{max} by noting that the steady state solution for the detailed shape of the lamellar solidification front seems to break down when λ becomes too large, and by identifying λ_{max} as the point at which this breakdown occurs. They have shown experimentally[8] that splittings occur under roughly the conditions predicted. Their calculation, however, is not fully self-consistent, nor is it obvious that the deformed solidification front remains dynamically stable all the way out to where the steady state solutions develop anomalies. Nash[9] has carried out a detailed self-consistent calculation of the steady state interface shape. However, the conditions under which breakdown occurs have not been investigated and the numerical results reported are only for the case of vanishing thermal gradient. Our current guess is that, in the limit of small temperature gradient G, λ_{max} scales like a stability length of the same form as λ_{min} in (2.3), so that Λ_{max} is a number of order unity which depends only on system parameters like volume fractions or ratios of interfacial energies. Λ_{max} should increase with increasing G; more specifically, we guess that Λ_{max} is an increasing function of the dimensionless group $GD/T_E v$.

3. MEAN-FIELD APPROXIMATION

To get a qualitative idea of what is happening in this model, we have found it useful to look at the following very simple mean-field approximation. Let $\bar{\Lambda}$ be some characteristic lamellar width to be determined self-consistently, and consider a single lamella of width Λ. If we assume that the lamellae on either side of Λ have widths $\bar{\Lambda}$, then (2.4) without noise becomes

$$\frac{d\Lambda}{d\tau} = 2(\bar{\Lambda} - 1)^2 - 2(\Lambda - 1)^2 \equiv -\frac{\partial \psi}{\partial \Lambda} \tag{3.1}$$

Here we have introduced a velocity potential in Λ space,

$$\psi(\Lambda) = \tfrac{2}{3}(\Lambda - 1)^3 - 2(\bar{\Lambda} - 1)^2(\Lambda - 1) \tag{3.2}$$

which has a stable minimum at $\Lambda = \bar{\Lambda}$ and an unstable maximum at $\Lambda = 2 - \bar{\Lambda}$. To include noise-induced fluctuations, we use (3.1) to write an equation of motion for the distribution function $n(\Lambda, \tau)$:

$$\frac{\partial n}{\partial \tau} = -\frac{\partial J}{\partial \Lambda} + s\delta(\Lambda - \Lambda_s) \tag{3.3}$$

where the Λ flux J is

$$J = -\frac{\partial \psi}{\partial \Lambda} n - 2\theta \frac{\partial n}{\partial \Lambda} \tag{3.4}$$

and s is the strength of the source of new lamellae being created at $\Lambda = \Lambda_s \equiv \Lambda_{\max}/2$ because of splitting at $\Lambda_{\max}$. We shall let the distribution function n be normalized so that

$$\int_0^{\Lambda_{\max}} n(\Lambda, \tau)\Lambda \, d\Lambda = 1 \tag{3.5}$$

Then the source strength s is the number of lamellae created per unit time per unit length of the system.

Using the termination and creation rules summarized in Fig. 2b, we can construct a steady state solution of Eqs. (3.3) and (3.4). Figure 6 shows the steady state $n(\Lambda)$ for some typical cases. As indicated in Fig. 6a, we have set $J = -J^-$ in the region $0 \leqslant \Lambda < \Lambda_s$ and $J = J^+$ in $\Lambda_s < \Lambda \leqslant \Lambda_{\max}$. The distribution $n(\Lambda)$ must vanish at $\Lambda = 0$ and $\Lambda = \Lambda_{\max}$, and must be continuous in value but have a discontinuity in its first derivative at $\Lambda = \Lambda_s$. The discontinuity in the flux at Λ_s is equal to the source strength s:

$$s = J^+ + J^- \tag{3.6}$$

and the splitting rule implies that

$$s = 2J^+ \tag{3.7}$$

Thus

$$J^+ = J^- = \tfrac{1}{2}s \tag{3.8}$$

We can integrate (3.4) to obtain

$$n(\Lambda > \Lambda_s) = \frac{s}{4\theta} e^{-\psi(\Lambda)/2\theta} \int_\Lambda^{\Lambda_{\max}} e^{\psi(\Lambda')/2\theta} \, d\Lambda' \tag{3.9a}$$

$$n(\Lambda < \Lambda_s) = \frac{s}{4\theta} e^{-\psi(\Lambda)/2\theta} \int_0^{\Lambda} e^{\psi(\Lambda')/2\theta} \, d\Lambda' \tag{3.9b}$$

Then the normalization condition (3.5) and the condition of continuity at Λ_s,

$$\lim_{\Lambda \to \Lambda_s} n(\Lambda > \Lambda_s) = \lim_{\Lambda \to \Lambda_s} n(\Lambda < \Lambda_s) \tag{3.10}$$

are sufficient to determine s and $\bar{\Lambda}$.

The only case in which the mean-field approximation might be taken seriously is when θ is small so that $n(\Lambda)$ is sharply peaked near $\Lambda = \bar{\Lambda}$. In that case, the integrands in (3.9) are also sharply peaked, and we can make simple estimates which allow us to evaluate s and $\bar{\Lambda}$ explicitly. We can see immediately, however, that the success of this procedure requires a sufficiently large $\Lambda_{\max}$ even in the limit of vanishingly small θ. Remember that the equation of motion (3.1) has a stable fixed point at $\Lambda = \bar{\Lambda}$ and an unstable one at $\Lambda = 2 - \bar{\Lambda}$. Lamellae with $\Lambda < 2 - \bar{\Lambda}$ move directly toward termination at $\Lambda = 0$ in this approximation. If $\Lambda_{\max}$ is so small that $\Lambda_s = \Lambda_{\max}/2$ is less than $2 - \bar{\Lambda}$, then all splittings lead to terminations and, at the very least, the nature of the small-θ solution changes dramatically. We shall see later that this is the mechanism which produces something like turbulence at small $\Lambda_{\max}$. For the moment, we shall simply assume $\Lambda_s > 2 - \bar{\Lambda}$.

Given this assumption, we can see that the peak in the integrand in (3.9a) is at $\Lambda = \Lambda_{\max}$, and that in (3.9b) it is at $2 - \bar{\Lambda}$. Thus

$$n(\Lambda > \Lambda_s) \approx \frac{s}{2\psi'(\Lambda_{\max})} \exp\left[\frac{\psi(\Lambda_{\max}) - \psi(\Lambda)}{2\theta} \right] \times \left\{ 1 - \exp\left[\frac{\psi'(\Lambda_{\max})}{2\theta} (\Lambda - \Lambda_{\max}) \right] \right\} \tag{3.11a}$$

and

$$n(\Lambda < \Lambda_s) \approx \frac{s}{4} \left[\frac{4\pi}{\theta |\psi''(2 - \Lambda)|} \right]^{1/2} \exp\left[\frac{\psi(2 - \bar{\Lambda}) - \psi(\Lambda)}{2\theta} \right] \tag{3.11b}$$

The continuity condition (3.10), after a little algebra, yields

$$\bar{\Lambda} \approx \frac{1}{2}(1 + \Lambda_{\max}) - \frac{\theta}{3(\Lambda_{\max} - 1)^2} \ln\left[\frac{9\pi(\Lambda_{\max} - 1)^3}{8\theta} \right] \tag{3.12}$$

The corresponding estimate for s, obtained by using (3.11a) in the normalization condition (3.5) and making the obvious Gaussian approximation, is

$$s \approx \frac{6}{(1 + \Lambda_{\max})} \left[\frac{(\Lambda_{\max} - 1)^5}{2\pi\theta} \right]^{1/2} \exp\left[-\frac{1}{3\theta} (2\bar{\Lambda} + \Lambda_{\max} - 3)(\Lambda_{\max} - \bar{\Lambda})^2 \right]$$
$$\propto \exp\left[-\frac{1}{6\theta} (\Lambda_{\max} - 1)^3 \right] \tag{3.13}$$

Using (3.11a) for $n(\Lambda)$, the mean-square deviation $\langle \delta\Lambda^2 \rangle$ in the Gaussian approximation is

$$\langle \delta\Lambda^2 \rangle \approx \frac{\theta}{\psi''(\bar{\Lambda})} \tag{3.14}$$

One interesting feature of these results is that the characteristic lamellar width $\bar{\Lambda}$, in the limit of small θ, occurs halfway between $\Lambda_{\max}$ and 1. The steady state configuration quite simply must balance the rates of splittings and terminations, and it does this by choosing a Λ which is equidistant from both ends of the range of allowed, stable values. The only vestige of the marginal-stability mechanism is the second term on the right-hand side of (3.12) which describes a θ-dependent shift toward the dynamical instability at $\Lambda = 1$. A second feature of interest is that the small-θ relation, $\bar{\Lambda} \cong (1 + \Lambda_{\max})/2$, when inserted into the steady state criterion $\Lambda_s = \Lambda_{\max}/2 > 2 - \bar{\Lambda}$, yields a lower bound for $\Lambda_{\max}$. Specifically, $\Lambda_{\max} \gtrsim 1.5$. Although differentially stable states exist in this model at any uniform Λ greater than 1, our mean-field analysis indicates that these states may be unstable against finite-amplitude perturbations if $\Lambda_{\max}$ is too small.

The mean-field equations (3.5), (3.9), and (3.10) can easily be solved numerically, that is, by direct numerical integration of (3.9) without making the small-θ approximation. The significance of going beyond small θ is questionable. However, it turns out that the "exact" mean-field results compare fairly well with direct numerical simulation of the caricature, and that comparison by itself is of some interest. We shall present both kinds of numerical results together in the next section.

4. NUMERICAL SIMULATION

Our eutectic caricature lends itself readily to numerical simulation; indeed, it was designed with that in mind.

We have used the following temporal discretization of the (already spatially discrete) equations of motion (2.4):

$$\frac{\Lambda_i^{M+1} - \Lambda_i^M}{\Delta\tau} = (\Delta_{i+1}^{M+1} - 1)(\Lambda_{i+1}^M - 1) - 2(\Lambda_i^{M+1} - 1)(\Lambda_i^M - 1) + (\Lambda_{i-1}^{M+1} - 1)(\Lambda_{i-1}^M - 1) + \eta_i^M - \eta_{i-1}^M \tag{4.1}$$

where the superscripts M, $M + 1$ label time steps taken in units $\Delta\tau$. This implicit scheme has allowed us to use large time steps $\Delta\tau$ (of order 10^{-1}) under most circumstances. The reflecting boundary conditions stated preceding Eq. (2.6) are physically realistic in that they simulate rigid edges. They also speed the computation by making it possible to obtain the Λ_i^{M+1} from the Λ_i^M by inversion of a simple banded matrix. (Periodic boundary

conditions would have permitted sidewise drift of the array as a whole, and would have required a more time-consuming matrix inversion.) The noise source $\eta_i(\tau)$ has been simulated by writing

$$\eta_i^M = \eta \alpha_i^M \tag{4.2}$$

where α_i^M is a random number in the interval $[-1, 1]$ chosen separately for each i, M and

$$\theta = \tfrac{1}{3}\eta^2 \Delta\tau \tag{4.3}$$

where θ is the effective temperature defined in (2.5).

In our simulation experiments, we generally have started with a set of Λ_i which are random numbers in some interval $[a, b]$ and then have computed the time evolution by iterating (4.1). Quantities monitored during this evolution include the average spacing

$$\langle \Lambda \rangle = \frac{L}{N} \tag{4.4}$$

the mean square deviation

$$\langle \delta\Lambda^2 \rangle = \frac{1}{N} \sum_i (\Lambda_i - \langle \Lambda \rangle)^2 \tag{4.5}$$

and the cumulative numbers of terminations and splittings. Here, N is the instantaneous total number of lamellae and L is the constant length defined in (2.6). We also have recorded the lamellar widths $\Lambda_i(\tau)$ so as to be able to make real-time plots of the evolution of the lamellar array. At finite values of θ, we have always observed the system to relax into a steady state situation with time-dependent values of $\langle \Lambda \rangle$, $\langle \delta\Lambda^2 \rangle$, etc. independent of the initial configuration. All of the data presented below have been obtained for systems with $L \gtrsim 20$. We have checked and have failed to find any appreciabel L dependence of the above quantities for systems of this size.

Figure 3 is a graph of the steady state average spacing $\langle \Lambda \rangle$ as a function of $\Lambda_{\max}$ for various values of θ. At large $\Lambda_{\max}$ and small θ the results of the computer simulation are in good agreement with the corresponding mean-field values for the average spacing.

Both the source strength s, which can be identified as the average number of terminations or splittings per unit length per unit time, and the ratio $\langle \delta\Lambda^2 \rangle / \langle \Lambda \rangle^2$ are measures of the intensity of disorder in the system. These quantities are shown, again as functions of $\Lambda_{\max}$ and θ, in Figs 4 and 5. We find that $\langle \delta\Lambda^2 \rangle / \langle \Lambda \rangle^2$ predicted by mean-field theory agrees quite well with the computer simulation at small θ and large $\Lambda_{\max}$. For example, in Fig. 5 the slope of $\langle \delta\Lambda^2 \rangle / \langle \Lambda^2 \rangle$ vs θ at the origin for the curve $\Lambda_{\max} = 2.1$ is 0.34, while the corresponding mean-field value from Eq. (3.14)

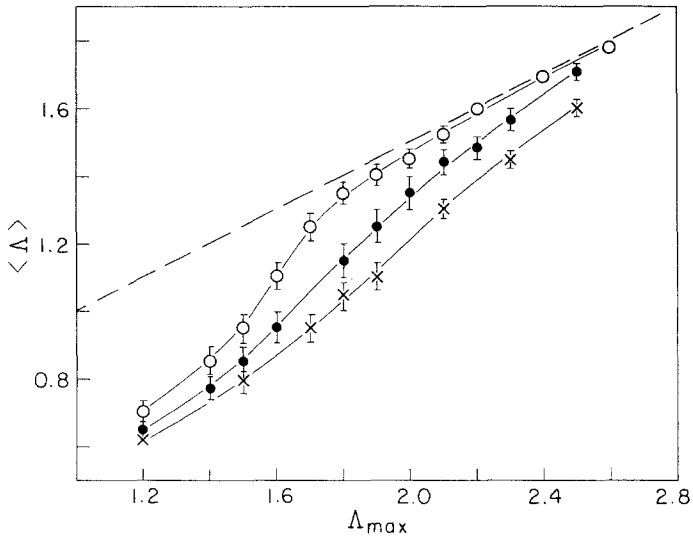

Fig. 3. Average lamellar spacing $\langle\Lambda\rangle$ as a function of Λ_{max} for three different values of θ. (Values of θ: ○, 0.03; ●, 0.13; ×, 0.30). The data points are obtained from computer simulation. Solid lines through the data points are drawn to guide the eye. The dashed line is the curve $\langle\Lambda\rangle = (1 + \Lambda_{max})/2$.

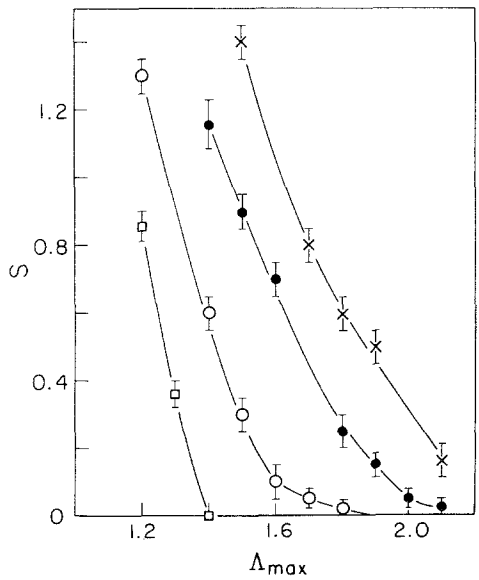

Fig. 4. Source strength s as a function of Λ_{max} for four different values of the noise strength θ, as obtained from the computer simulation. Solid lines are drawn to guide the eye. Values of θ: □, 0.00; ○, 0.03; ●, 0.13; ×, 0.30.

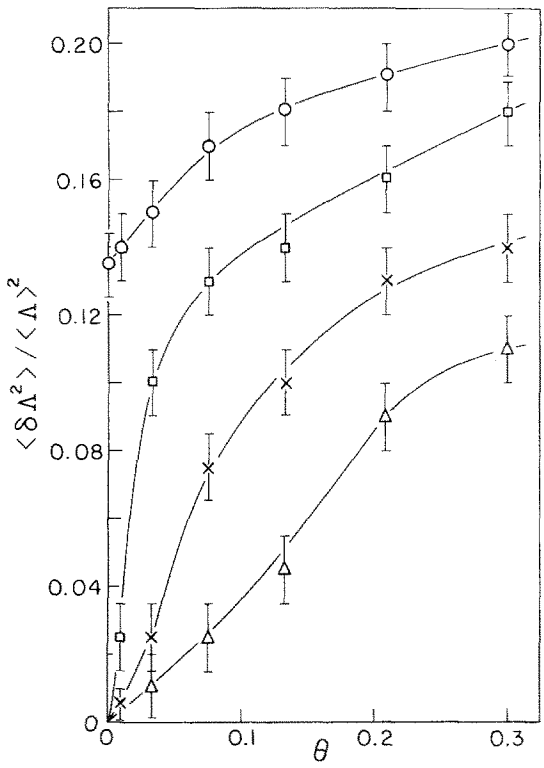

Fig. 5. Graph of the mean square deviation in the lamellar spacing, $\langle \delta\Lambda^2 \rangle / \langle \Lambda \rangle^2$, as a function of noise strength θ, for four different values of Λ_{max} (values of Λ_{max}: ○, 1.2; □, 1.5; ×, 1.8; △, 2.1). The data points are obtained from computer simulation, the solid lines are drawn to guide the eye.

is 0.38. Both figures show a sensitive dependence on Λ_{max} and, in particular, indicate that the external noise is increasingly amplified as Λ_{max} decreases. The most dramatic feature to emerge from these numerical experiments is that the disorder in the system seems to persist indefinitely for values of Λ_{max} less than some critical $\Lambda_c \cong 1.3$. This effect is shown quantitatively by the points marked $\theta = 0$ in the figures. We believe that here we are seeing the intrinsic chaotic behavior suggested by the breakdown of the mean-field theory for $\Lambda_{max} < 1.5$.

In Fig. 6 we plot the steady state distribution function $n(\Lambda)$, obtained from the computer simulation, for some typical cases. The histograms shown in the figure represent averages over several snapshots of the system in steady state. The snapshots are separated by a sufficiently large time

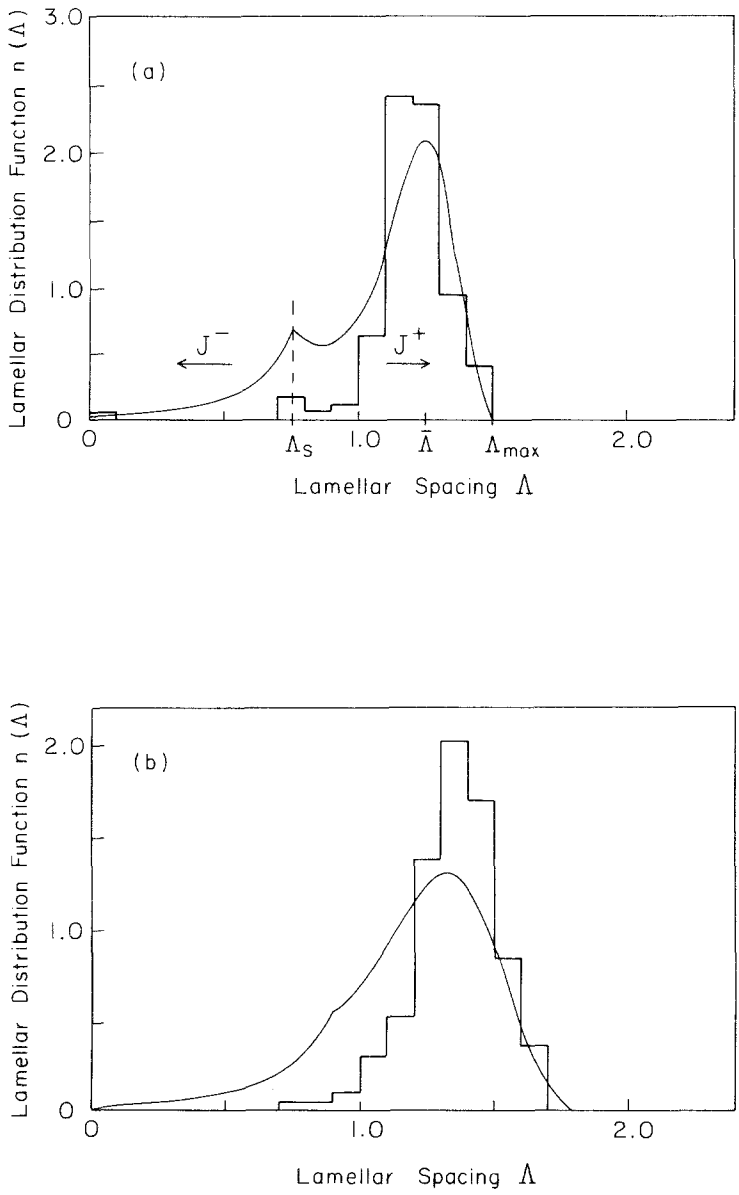

Fig. 6. Histograms of the steady state lamellar distribution function $n(\Lambda)$ as obtained from the computer simulation. The corresponding mean-field $n(\Lambda)$ is superimposed on each plot for comparison. (a) $\theta = 0.0083$, $\Lambda_{max} = 1.5$; (b) $\theta = 0.0333$, $\Lambda_{max} = 1.8$; (c) $\theta = 0.1333$, $\Lambda_{max} = 1.8$; (d) $\theta = 0.0333$, $\Lambda_{max} = 2.1$.

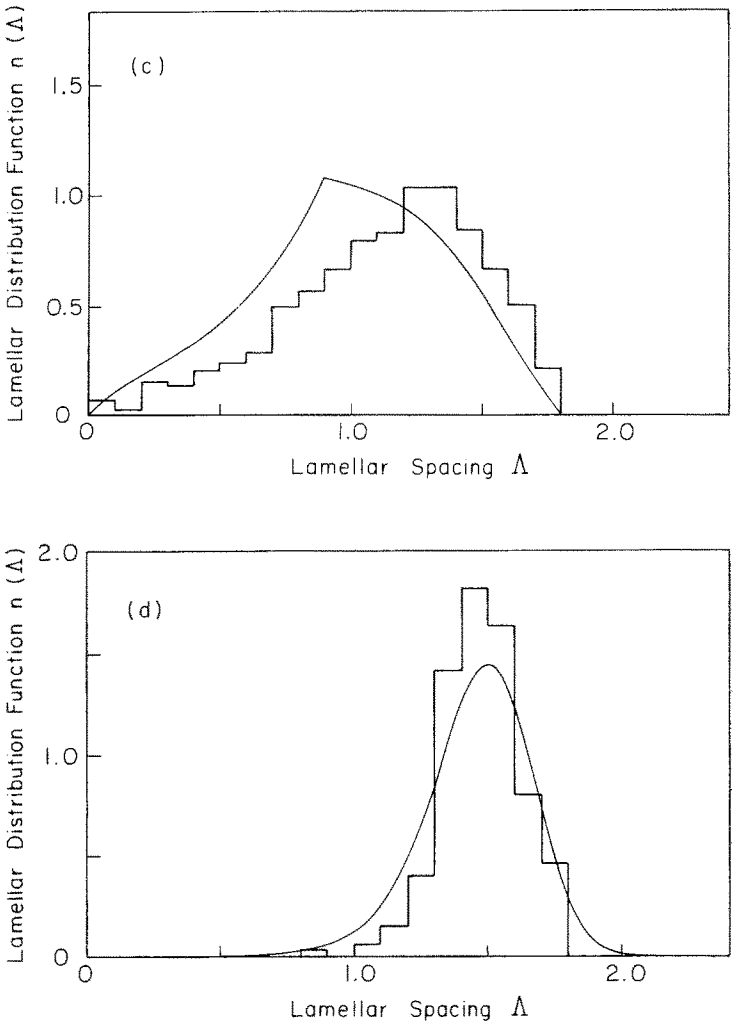

Fig. 6 (continued)

interval ($\cong 300$ time steps), so as to ensure that they are statistically independent. The corresponding mean-field distributions are superimposed on these plots for comparison. As mentioned above, the comparison is somewhat better than might have been expected at small θ and large Λ_{max}.

Figures 7–9 are pictures of the eutectic pattern as might be seen by direct observation of the system after solidification had taken place in the upward direction. That is, the lamellar widths are displayed along the

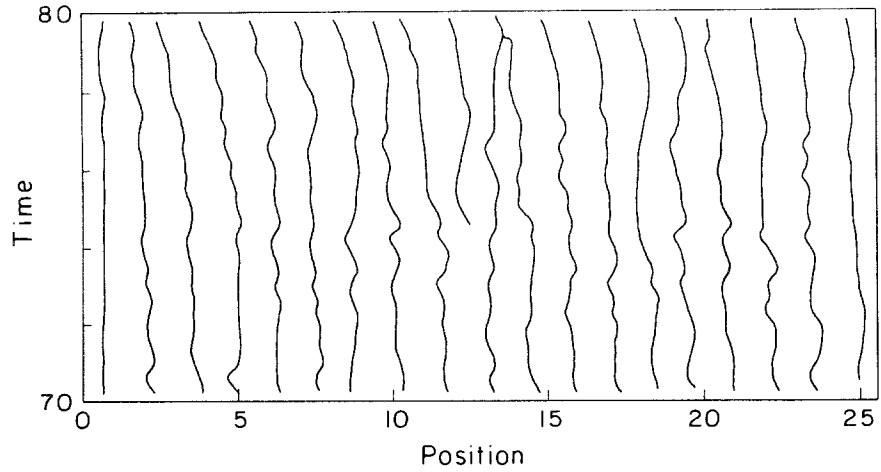

Fig. 7. Time evolution of the lamellar array. Steady state behavior at $\Lambda_{max} = 1.8$, $\theta = 0.048$.

horizontal axis and τ increases in the vertical direction. Figure 7 shows a normal steady state behavior, with occasional terminations and splittings, for $\Lambda_{max} = 1.8$ and $\theta = 0.048$. Figures 8 and 9 are both pictures of behavior with no external noise, $\theta = 0$. In Fig. 9, with $\Lambda_{max} = 1.3$, the initially disordered system has settled down into an oscillating mode in which a kink propagates from side to side and is reflected at the edges. Figure 9

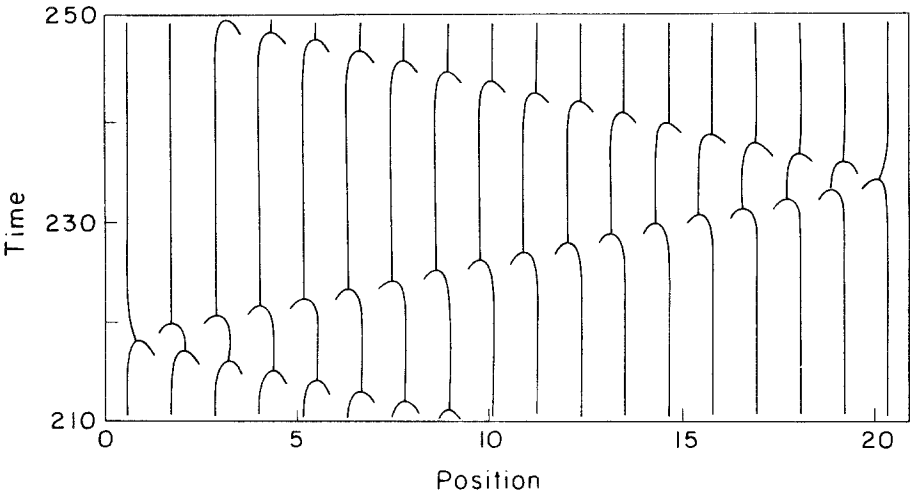

Fig. 8. Kink behavior at $\Lambda_{max} = 1.3$, $\theta = 0$.

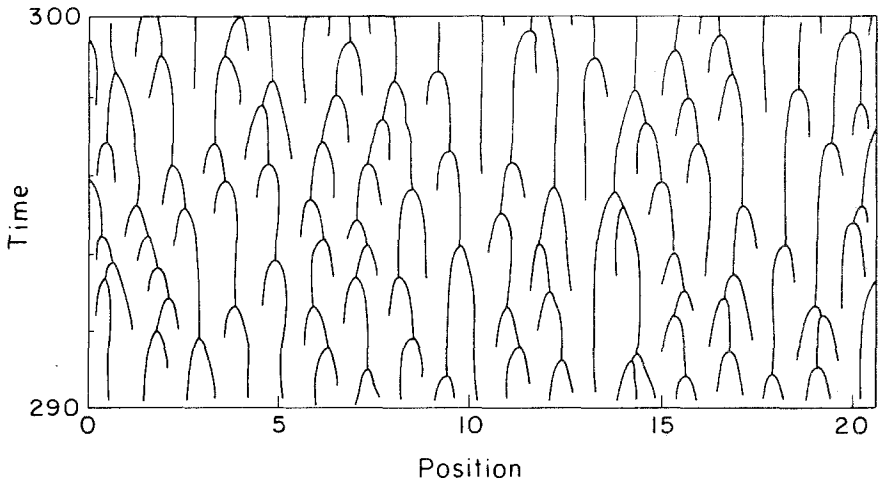

Fig. 9. Fully turbulent behavior at $\Lambda_{max} = 1.2$, $\theta = 0$.

shows what looks like fully turbulent behavior at $\Lambda_{max} = 1.2$. So far as we can tell, the latter two modes of behavior persist indefinitely.

ACKNOWLEDGMENT

This research was sponsored by a contract from the Division of Materials Sciences of the Department of Energy.

REFERENCES

1. K. A. Jackson and J. D. Hunt, *Trans. Met. Soc. AIME* **236**:1129 (1966).
2. G. Lesoult, *Ann. Chim. (Paris)* **5**:154 (1980).
3. J. S. Langer, *Phys. Rev. Lett.* **44**:1023 (1980).
4. V. Datye and J. S. Langer, *Phys. Rev. B* **24**:4155 (1981).
5. J. S. Langer, *Ann. N.Y. Acad. Sci.* **373**:179 (1981).
6. R. M. Jordan and J. D. Hunt, *Met. Trans.* **2**:3401 (1971).
7. J. van Suchtelen, private communication.
8. J. D. Hunt and K. A. Jackson, *Trans. Met. Soc. AIME* **236**:843 (1966).
9. G. E. Nash, *J. Cryst. Growth* **38**:155 (1977).